ARTICLES
https://doi.org/10.1038/s41561-017-0001-8
nature geoscience

Enhanced poleward propagation of storms under climate change

Talia Tamarin-Brodsky* and Yohai Kaspi

Earth's midlatitudes are dominated by regions of large atmospheric weather variability—often referred to as storm tracks—which influence the distribution of temperature, precipitation and wind in the extratropics. Comprehensive climate models forced by increased greenhouse gas emissions suggest that under global warming the storm tracks shift poleward. While the poleward shift is a robust response across most models, there is currently no consensus on what the underlying dynamical mechanism is. Here we present a new perspective on the poleward shift, which is based on a Lagrangian view of the storm tracks. We show that in addition to a poleward shift in the genesis latitude of the storms, associated with the shift in baroclinicity, the latitudinal displacement of cyclonic storms increases under global warming. This is achieved by applying a storm-tracking algorithm to an ensemble of CMIP5 models. The increased latitudinal propagation in a warmer climate is shown to be a result of stronger upper-level winds and increased atmospheric water vapour. These changes in the propagation characteristics of the storms can have a significant impact on midlatitude climate.

Extratropical storm tracks and the associated mobile weather systems that compose them play a key role in the global atmospheric circulation, as they transport heat and moisture poleward. The low-pressure cyclonic storms are often associated with intense precipitation and winds, and therefore their frequency, intensity and paths have a significant effect on weather and climate. The storm tracks can be defined either using an Eulerian approach, as regions of enhanced eddy activity[1] (for example, eddy kinetic energy (EKE)), or alternatively using a Lagrangian approach, as regions of high track density (Fig. 1a) and mean intensity (Fig. 1a, black contours)[2]. The Lagrangian approach separates the cyclones and anti-cyclones that compose the storm track and gives information about their temporal evolution, and is therefore adopted for the current study.

The storm tracks' response to climate change has been a focus of research in recent years[3–8], as even small deviations in the strength or location of the storm tracks can result in significant changes in the regional climate and hydrological cycle. Although there are still large uncertainties in the projected storm track response, especially regionally[3,5,6], it is now largely accepted that under global warming the storm tracks shift poleward and expand upward, and the total number of cyclonic storms decreases[3,5,7,9–13], although the frequency of extreme cyclones is projected to increase in the Southern Hemisphere (SH)[14,15]. Reanalysis-based studies suggest that a similar trend has already been observed over the last half of the twentieth century[3,16,17]. The poleward shift is a relatively robust prediction, achieved also in simplified models[18–21], and is especially clear in the SH (Fig. 1e).

The poleward shift of storm tracks

Many mechanisms have been proposed to explain the poleward shift, including changes in near-surface meridional temperature gradients and the associated terminus of the Hadley circulation[9,22], increased subtropical static stability[18,23], changes in tropopause height[24], enhanced tropical heating[25] and changes in sea surface temperature[19,26–28]. The dominant underlying mechanism is still debated, and several of these mechanisms may act in parallel. In addition, the existence of competing thermodynamic effects makes the predictions even more challenging[21]. For example, while the warming of the upper tropical troposphere increases the upper-level temperature gradient and shifts the storm tracks poleward, Arctic surface warming decreases the low-level temperature gradient and therefore acts to shift the storm tracks equatorward[25]. These arguments all imply changes in the latitudinal position of baroclinicity, which in turn implies a change in the latitudinal position of the storm track genesis regions. This study, however, highlights a different aspect of the poleward shift. It is shown here that in addition to a shift in the genesis latitude of the storms, it is also the storms themselves that propagate more poleward until they reach their peak intensity. This is potentially related to other proposed mechanisms for the poleward shift, which involve changes in the eddy phase speed spectra, wave breaking and eddy length scales[24,29–32].

Enhanced poleward motion of cyclones was found previously in idealized global-warming-like experiments of simplified aquaplanet general circulation models (GCMs)[28,33]. Here we show that this is a robust response that appears also in a comprehensive multi-GCM ensemble, and suggest that it can explain a large fraction of the overall observed poleward shift. This is achieved by analysing 20 Coupled Model Intercomparison Project 5 (CMIP5) ensemble members (see Supplementary Table 1) forced by the Representative Concentration Pathway 8.5 emissions scenario[34], and applying a storm-tracking algorithm[35] on each one of the ensemble members. The projected changes are obtained by subtracting the historical simulations (years 1980–1999) from the projected simulations (years 2080–2099). The full details of the tracking method are given in the Methods.

The projected low-level (850 hPa) track density change during Northern Hemisphere (NH) winter time (December–February, DJF) shows a poleward shift of the storm tracks, mostly in the SH (Fig. 1e). In the NH (Fig. 1c), this picture is further complicated due to continents that break the zonal (east–west) symmetry. There is an indication of a strengthening (weakening) of the track density on the poleward (equatorward) side of the storm tracks, and also a strengthening in the downstream regions of the storm tracks; that is, close to the northeastern ocean boundaries. Consistent with

Weizmann Institute of Science, Department of Earth and Planetary Sciences, Rehovot 76100, Israel. *e-mail: talia.tamarin@weizmann.ac.il

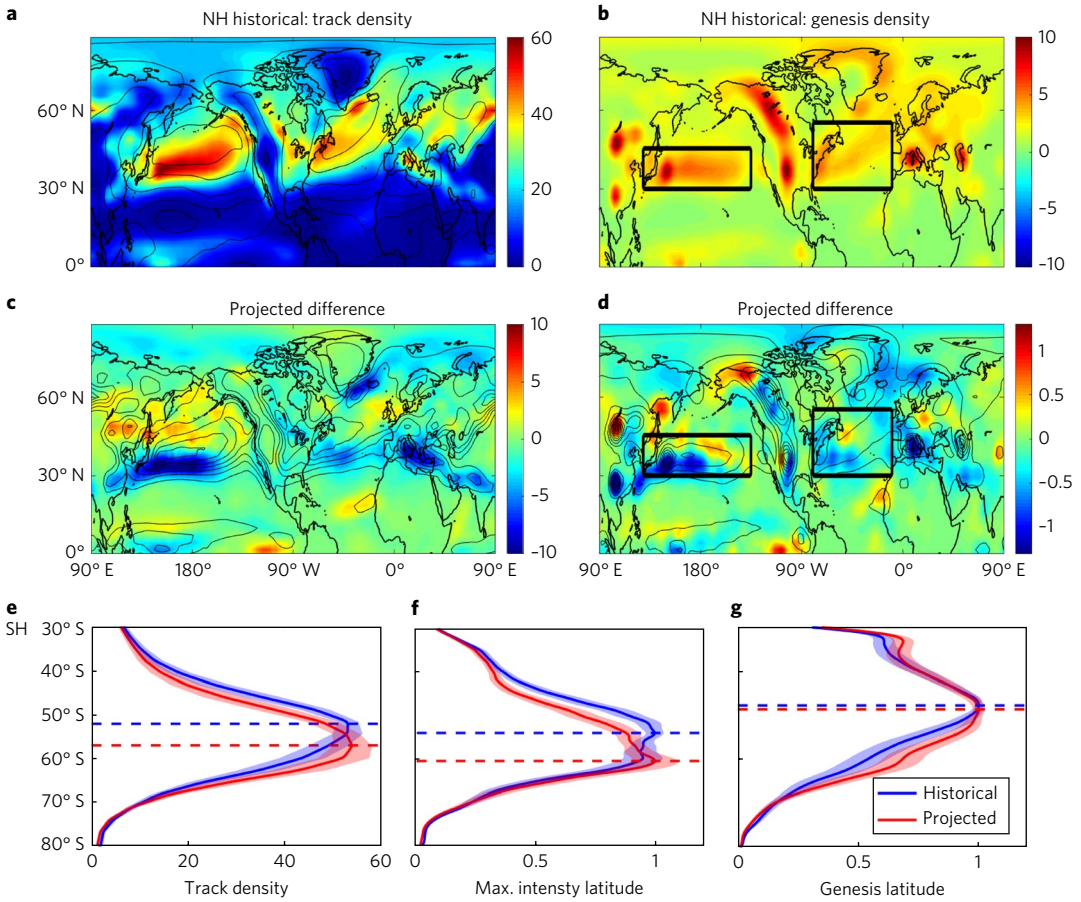

Fig. 1 | Ensemble-mean CMIP5 tracking statistics for the historical (1980–1999) storm tracks and the projected changes (2080–2099 minus historical). **a**–**d**, Historical low-level (850 hPa) cyclone track density (**a**) and genesis density (**b**) in the NH, and the corresponding projected changes (with historical values in black contours) (**c**,**d**). Black contours in **a** denote the historical mean intensity. Densities are normalized by 10^6 km^2 per season. **e**–**g**, SH zonally averaged track density (**e**), normalized PDF distribution of latitude of maximum intensity (**f**), and genesis latitude of the cyclones (**g**) for the historical (projected) runs in blue (red), where dashed lines denote the latitude of maximum PDF. The PDFs are obtained using a kernel fitting for all cyclones generated between latitudes 30° S and 70° S, and the shading denotes the 95% confidence interval.

observational data[2], the ensemble-averaged genesis density of cyclones in the historical runs (Fig. 1b) picks up the genesis regions associated with the baroclinic growth of the Pacific and Atlantic storm tracks, to the east of Japan and off the eastern coast of the United States, respectively (black boxes in Fig. 1b,d). These coincide with regions of strong cyclone growth rates, as a result of the large temperature contrasts between the cold continents and the warmer ocean currents. The projected genesis density changes in the regions marked by the boxes (Fig. 1d) show mainly a weakening of the genesis densities (consistent with the overall decrease in the total number of cyclones), with some strengthening on the poleward side and in the downstream region of the Pacific storm track.

In the SH, the latitude of maximum zonally averaged cyclone track density (Fig. 1e) shifts poleward by about 4.9° in latitude. Consistent with that, the peak of the normalized probability density function (PDF) of the cyclones' maximum intensity latitude shifts poleward by about 6.5° (Fig. 1f) in latitude. The projected shift in the PDF of the cyclones' maximum genesis latitude (Fig. 1g) is smaller, approximately 0.9° in latitude; however, there is a clear poleward expansion of the genesis region, probably associated with the projected shift in baroclinicity[9]. Some genesis regions are constrained by topography and are therefore not expected to change, which is possibly why a smaller shift in the genesis latitude is observed.

Projected changes in cyclonic tracks

An example model. The tracks of all the cyclonic relative vorticity features in the historical runs during DJF, which first originated in the genesis regions marked by the black boxes, are plotted in Fig. 2 for an example model (HadGEM-CC), for the NH (Fig. 2a) and the SH (Fig. 2b). The magenta and black arrows show the average starting location and displacements (until maximum intensity) of cyclones within each genesis region, for the historical and projected runs, respectively. In the Pacific storm track, the averaged cyclone in the historical (projected) runs is generated at latitude 37° N (37.3° N) and propagates 6.5° (8.2°) poleward until it reaches maximum intensity. Hence, the latitude of maximum cyclone intensity in the Pacific shifts poleward by about 2.0°, from which 85% is explained by the enhanced latitudinal displacements. In the Atlantic storm track, there is an overall poleward shift of 1.4° in the latitude of maximum cyclone intensity, from which 42% is explained by the enhanced latitudinal displacements. For the SH storm track, the tracks of the 100 strongest cyclones per year during DJF that were generated between latitudes 30° S and 70° S are plotted in Fig. 2. The averaged cyclone in the historical (projected) runs is generated at latitude 47.2° S (48.6° S) and propagates 8.1° (9.5°) poleward until it reaches maximum intensity. Hence, the averaged starting point of cyclones in the SH shifts by 1.4° poleward, but the averaged cyclone also propagate 1.4° in latitude more poleward, which explains 50% of the overall shift.

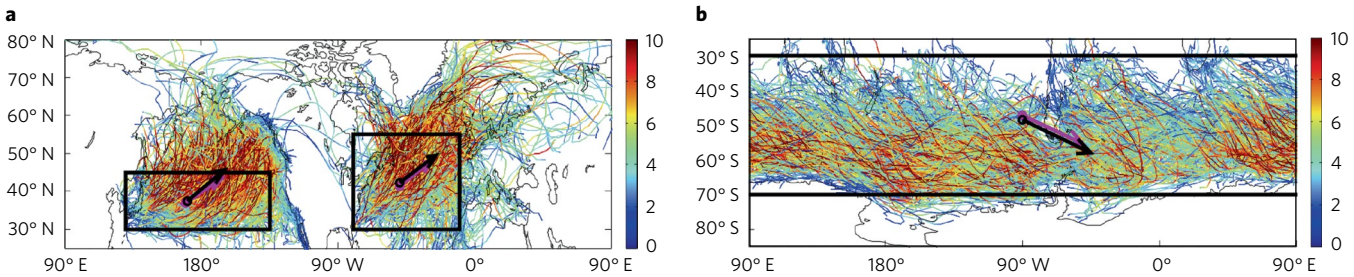

Fig. 2 | The historical (1980–1999) tracks of the low-level cyclones (850 hPa) for an CMIP5 example model, HadGEM-CC (model number 10 from Supplementary Table 1). Shown are all of the cyclones that were generated in the genesis regions marked by the black boxes in the NH (**a**), and the 100 most intense cyclones per year during DJF generated between latitude 30° S and 70° S in the SH (**b**). The magenta (black) arrows show the averaged cyclonic track (until maximum intensity) in the historical (projected) runs, for each genesis region. Colour indicates the intensity of the storm (measured in vorticity and scaled by 10^{-5} s^{-1}).

Multi-GCM ensemble. The results of all the CMIP5 models used in this study (see Supplementary Table 1) for DJF are shown in Fig. 3, for the projected differences in the mean starting latitude of the cyclonic storms (left column), latitude of maximum intensity (middle column) and the overall latitudinal displacement until maximum intensity (right column). Most models agree on a statistically significant increase in the average genesis latitude of the cyclonic storms in the Pacific (Fig. 3d) and SH (Fig. 3g) storm tracks, and less agreement exists for the Atlantic storm track (Fig. 3a). However, in all three storm tracks, almost all models agree on a statistically significant poleward shift in the mean latitude of cyclone peak intensity (middle column). The ensemble

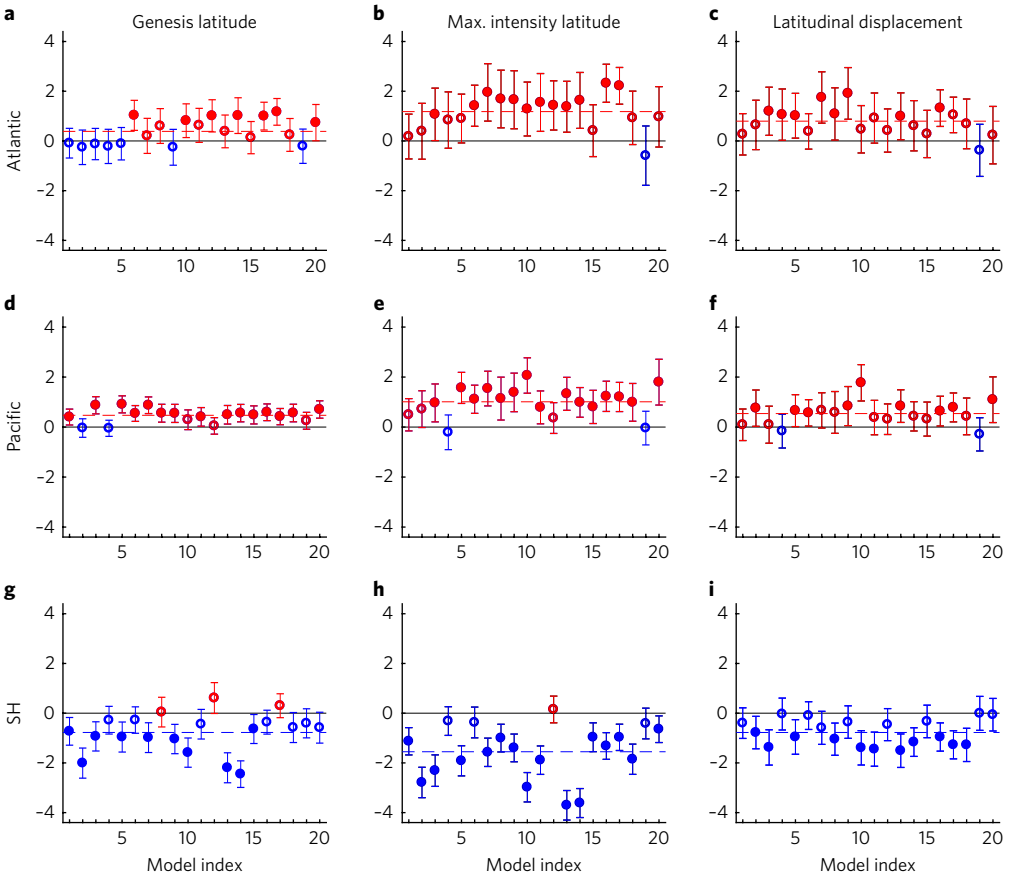

Fig. 3 | Model-to-model variations in the projected differences of cyclonic tracks. The mean genesis latitude, maximum intensity latitude and overall latitudinal displacements until maximum intensity for the Atlantic storm track, the Pacific storm track and the SH storm track. Each dot represents a model, where the model index on the abscissa is given in accordance with the list in Supplementary Table 1. The averages are calculated for all cyclones that first appeared in the genesis regions described in the text, for the years 1980–1999 (2080–2099) in the historical (projected) runs. Red (blue) denotes negative (positive) values, and dashed horizontal lines show the ensemble mean averages. The error bars denote the 95% confidence interval, and dots that are significant at the 5% level are filled.

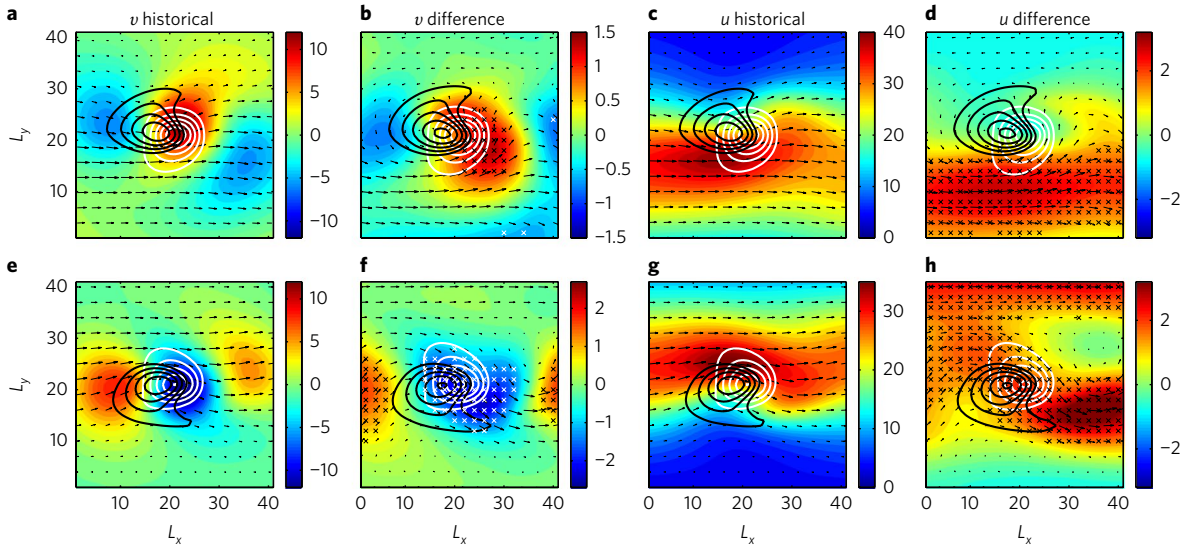

Fig. 4 | Upper-level (250 h Pa) velocity composites produced by tracking the low-level (850 hPa) cyclonic vorticity features. a–h, Meridional velocity (**a**,**e**) and its projected changes (**b**,**f**), and zonal velocity (**c**,**g**) and its projected changes (**d**,**h**), for the NH (**a**–**d**) and the SH (**e**–**h**), for all cyclones identified from latitude 30° N or 30° S and poleward, respectively. The composites of sea-level pressure anomaly are shown in white contours, upper-level vorticity in black contours, and the upper-level velocity field is indicated by arrows, for the historical (**a**,**e**,**c**,**g**) and the projected (**b**,**f**,**d**,**h**) runs, for each hemisphere. Regions where 2/3 of the models (68%) agree on statistically significant increases (decreases) on the 5% level are marked by the white (black) crosses. The sea-level pressure outmost contour is equal to −2 hPa, with contour intervals equal to −1.5 hPa. The NH (SH) vorticity outmost contour is equal to $17\times10^{-6}\,s^{-1}$ ($-17\times10^{-6}\,s^{-1}$), with contour intervals equal to $7\times10^{-6}\,s^{-1}$ ($-9.5\times10^{-6}\,s^{-1}$).

mean change (dashed line in each panel) predicts a much larger shift in the latitude of maximum intensity than in the mean starting latitude. Indeed, in all three storm tracks, almost all models show an increased latitudinal displacement of cyclones until maximum intensity (right column), which is statistically significant in about half of the models. Hence, the cyclones are not only formed more poleward in a warmer climate, but they also propagate more poleward until they reach their peak intensity. Similar results are obtained for the SH winter (not shown). In addition, the longitudinal displacements of cyclones until peak intensity (Supplementary Fig. 1a,c,e) increase in the projected runs, but this is less robust. There is no significant difference in the lifetime of the storms across the Pacific and Atlantic storm tracks (Supplementary Fig. 1b,d), but a more robust response is observed for the SH (Supplementary Fig. 1f). There, the cyclones not only translate to larger distances, but also live shorter and therefore propagate faster. The overall averaged poleward shift in the latitude of maximum cyclone intensity (from all models) is 1.0° in the Pacific, 1.2° in the Atlantic, and 1.6° in the SH, from which 0.5° (50%), 0.8° (66%) and 0.7° (43%) is due to enhanced latitudinal drift of cyclones in each storm track, respectively.

Mechanisms for enhanced poleward propagation

Two main processes contribute to the poleward propagation of mid-latitude cyclones. First, during their growth stage, the cyclones are located to the east of an upper-level wave trough; hence, they reside in a region of strong poleward velocity at upper levels[36–38] (Fig. 4a,e). This poleward meridional velocity is induced at low levels, and is thus continuously advecting the low-level cyclones poleward[36,37] (Supplementary Figs. 4 and 5). This was shown previously in an idealized GCM using potential vorticity (PV) inversion[37,38], where PV is the absolute circulation of a fluid parcel enclosed between two isentropic surfaces[39], and is conserved following the parcel for an adiabatic and inviscid process. The PV inversion is also demonstrated in the Supplementary Information for an example CMIP5 model, MPI-ESM-LRM (Supplementary Fig. 5). Second, latent heating associated with the condensation of upward rising air tends to maximize at the poleward–eastern side of the cyclone[37]. The resulting mid-tropospheric warming acts to tighten the isentropes below the heating, and to stretch them above the heating. This enhances the upward motion and therefore the mass convergence and cyclonic circulation at low levels[40], and thus contributes to the poleward and eastward propagation of the low-level cyclones[37] (Supplementary Fig. 4b).

Both mechanisms for poleward motion of cyclones are expected to intensify in a warmer climate. First, the advection by the upper-level winds is intensified as a result of the strengthening of the upper-level flow. Figure 4 shows composites of the upper-level velocities, produced by tracking the 850 hPa relative vorticity features from all of the models. In both hemispheres, there is an enhancement of the upper-level meridional velocity in the region where the minimum mean sea-level pressure anomaly is located (Fig. 4b,d). A stronger upper-level meridional velocity also implies that the velocity induced at low levels is stronger, hence more poleward advection[37] (see Supplementary Fig. 5). Indeed, models that project a stronger increase in upper-level meridional wind speed also tend to project a stronger poleward shift, mostly in the SH (Supplementary Fig. 3). The interpretation of this correlation is supported by a full PV tendency budget for an example CMIP5 model, MPI-ESM-LRM, which shows explicitly the enhancement of the meridional advection in the projected simulation (Supplementary Fig. 4), as well as the induced low-level advection (Supplementary Fig. 5).

The upper-level zonal flow is also intensified in the projected composites, although mostly to the south of the cyclone in the NH. In the SH, there is an enhancement of the composite zonal flow in the region where the cyclone is located, consistent with previous studies that found an enhancement of the jet speed in the SH[41]. The intensification of the upper-level velocities and vorticity (Fig. 4b,f,d,h) is consistent with the enhanced upper-level EKE found in the projected runs of CMIP5[5,9]. This is potentially related to the projected increase in the upper-level baroclinicity found in previous studies[9], which implies more wave growth, and therefore

one can expect to find stronger upper-level wave amplitudes and associated velocities.

The second mechanism for poleward propagation, which is related to latent heating, is expected to intensify due to the increase in atmospheric water vapour content in a warmer climate[42]. More atmospheric moisture also leads to increased cyclone precipitation[43]; hence, more latent heating is expected to occur in a warmer climate. This can affect the low-level cyclones, since the mid-tropospheric heating will enhance the ascending air of the cyclone and therefore the cyclonic circulation at low levels. Since latent heating and vertical motions tend to maximize in the poleward–eastern side of the cyclone, where warm and moist air travels poleward and upward, this will contribute even further to the eastward and poleward propagation of the low-level cyclones[37]. This is shown to occur in the example model (Supplementary Fig. 4), where the low-level diabatically produced PV tendency due to latent heating is shown to intensify in the projected composites.

Shift versus tilt of midlatitude storm tracks

Enhanced latitudinal displacement of cyclones until maximum intensity necessarily implies a poleward extension of the storm tracks, regardless of any poleward shift in the genesis latitude of the storms. For example, in a zonally symmetric storm track (such as the SH storm track), if cyclones reach their peak intensity more poleward, then the track density, mean intensity and other storm tracks measures such as EKE will all intensify at higher latitude, giving an overall poleward extension. In a localized storm track (for example, the Pacific and Atlantic storm tracks in the NH), one must distinguish between the shift and the tilt of the storm track. While enhanced poleward motion of cyclones in a localized storm track implies a poleward extension, it does not necessarily imply a more titled storm track. For example, if the latitudinal and longitudinal displacements increase similarly, then the main response is an elongation of the storm track toward the tilted downstream region. Such changes in cyclone tracks can have a significant impact on local climate and weather in the midlatitudes, especially in regions close to the northeastern oceanic boundaries.

Methods

Methods, including statements of data availability and any associated accession codes and references, are available at https://doi.org/10.1038/s41561-017-0001-8.

Received: 16 March 2017; Accepted: 3 October 2017;
Published online: 13 November 2017

References

1. Blackmon, M., Wallace, J., Lau, N. & Mullen, S. An observational study of the Northern Hemisphere wintertime circulation. *J. Atmos. Sci.* **34**, 1040–1053 (1977).
2. Hoskins, B. & Hodges, K. New perspectives on the Northern Hemisphere winter storm tracks. *J. Atmos. Sci.* **59**, 1041–1061 (2002).
3. Ulbrich, U., Leckebusch, G. C. & Pinto, J. G. Extra-tropical cyclones in the present and future climate: a review. *Theor. Appl. Climatol.* **96**, 117–131 (2009).
4. O'Gorman, P. A. Understanding the varied response of the extratropical storm tracks to climate change. *Proc. Natl Acad. Sci. USA* **107**, 19176–19180 (2010).
5. Chang, E. K. M., Guo, Y. & Xia, X. CMIP5 multimodel ensemble projection of storm track change under global warming. *J. Geophys. Res.* **117**, D23118 (2012).
6. Harvey, B. J., Shaffrey, L. C., Woollings, T. J., Zappa, G. & Hodges, K. I. How large are projected 21st century storm track changes? *Geophys. Res. Lett.* **39**, L18707 (2012).
7. Zappa, G., Shaffrey, L. C. & Hodges, K. I. The ability of CMIP5 models to simulate North Atlantic extratropical cyclones. *J. Clim.* **26**, 5379–5396 (2013).
8. Shaw, T. A. et al. Storm track processes and the opposing influences of climate change. *Nat. Geosci.* **9**, 656–664 (2016).
9. Yin, J. H. A consistent poleward shift of the storm tracks in simulations of 21st century climate. *Geophys. Res. Lett.* **32**, L18701 (2005).
10. Bengtsson, L., Hodges, K. I. & Roeckner, E. Storm tracks and climate change. *J. Clim.* **19**, 3518–3543 (2006).
11. Bengtsson, L., Hodges, K. I. & Keenlyside, N. Will extratropical storms intensify in a warmer climate? *J. Clim.* **22**, 2276–2301 (2009).
12. Catto, J. L., Shaffrey, L. C. & Hodges, K. I. Northern Hemisphere extratropical cyclones in a warming climate in the HiGEM high-resolution climate model. *J. Clim.* **24**, 5336–5352 (2011).
13. Mizuta, R. Intensification of extratropical cyclones associated with the polar jet change in the CMIP5 global warming projections. *Geophys. Res. Lett.* **39**, L19707 (2012).
14. Lambert, S. J. & Fyfe, J. C. Changes in winter cyclone frequencies and strengths simulated in enhanced greenhouse warming experiments: results from the models participating in the IPCC diagnostic exercise. *Clim. Dyn.* **26**, 713–728 (2006).
15. Chang, E. K. M. Projected significant increase in the number of extreme extratropical cyclones in the Southern Hemisphere. *J. Clim.* **30**, 4915–4935 (2017).
16. McCabe, G. J., Clark, M. P. & Serreze, M. C. Trends in northern hemisphere surface cyclone frequency and intensity. *J. Clim.* **14**, 2763–2768 (2001).
17. Fyfe, J. C. Extratropical southern hemisphere cyclones: harbingers of climate change? *J. Clim.* **16**, 2802–2805 (2003).
18. Lu, J., Chen, G. & Frierson, D. M. W. The position of the midlatitude storm track and eddy-driven westerlies in aquaplanet AGCMs. *J. Atmos. Sci.* **67**, 3984–4000 (2010).
19. Graff, L. S. & LaCasce, J. H. Changes in the extratropical storm tracks in response to changes in SST in an AGCM. *J. Clim.* **25**, 1854–1870 (2012).
20. Mbengue, C. & Schneider, T. Storm track shifts under climate change: what can be learned from large-scale dry dynamics. *J. Clim.* **26**, 9923–9930 (2013).
21. Shaw, T. A. & Voigt, A. What can moist thermodynamics tell us about circulation shifts in response to uniform warming? *Geophys. Res. Lett.* **43**, 4566–4575 (2016).
22. Mbengue, C. & Schneider, T. Storm-track shifts under climate change: toward a mechanistic understanding using baroclinic mean available potential energy. *J. Atmos. Sci.* **74**, 93–110 (2017).
23. Lu, J., Vecchi, G. A. & Reichler, T. Expansion of the Hadley cell under global warming. *Geophys. Res. Lett.* **34**, L06805 (2007).
24. Lorenz, D. J. & DeWeaver, E. T. Tropopause height and zonal wind response to global warming in the IPCC scenario integrations. *J. Geophys. Res.* **112**, D10119 (2007).
25. Butler, A. H., Thompson, D. W. J. & Heikes, R. The steady-state atmospheric circulation response to climate change-like thermal forcings in a simple general circulation model. *J. Clim.* **23**, 3474–3496 (2010).
26. Caballero, R. The dynamic range of poleward energy transport in an atmospheric general circulation model. *Geophys. Res. Lett.* **32**, L02705 (2005).
27. Kodama, C. & Iwasaki, T. Influence of the SST rise on baroclinic instability wave activity under an aquaplanet condition. *J. Atmos. Sci.* **66**, 2272–2287 (2009).
28. Graff, L. S. & LaCasce, J. H. Changes in cyclone characteristics in response to modified SSTs. *J. Clim.* **27**, 4273–4295 (2014).
29. Kushner, P. J. & Polvani, L. M. Stratosphere-troposphere coupling in a relatively simple AGCM: impact of the seasonal cycle. *J. Clim.* **19**, 5721–5727 (2006).
30. Chen, G. & Held, I. M. Phase speed spectra and the recent poleward shift of Southern Hemisphere surface westerlies. *Geophys. Res. Lett.* **34**, L21805 (2007).
31. Kidston, J., Dean, S. M., Renwick, J. A. & Vallis, G. K. A robust increase in the eddy length scale in the simulation of future climates. *Geophys. Res. Lett.* **37**, L03806 (2010).
32. Rivière, G. A dynamical interpretation of the poleward shift of the jet streams in global warming scenarios. *J. Atmos. Sci.* **68**, 1253–1272 (2011).
33. Tamarin, T. & Kaspi, Y. The poleward shift of storm tracks under global warming: a Lagrangian perspective. *Geophys. Res. Lett.* **44**, L073633 (2017).
34. Taylor, K., Stouffer, R. & Meehl, G. An overview of CMIP5 and the experiment design. *Bull. Am. Meteorol. Soc.* **93**, 485–498 (2012).
35. Hodges, K. I. Feature tracking on the unit sphere. *Mon. Weather Rev.* **123**, 3458–3465 (1995).
36. Coronel, B., Ricard, D., Rivière, G. & Arbogast, P. Role of moist processes in the tracks of idealized mid-latitude surface cyclones. *J. Atmos. Sci.* **72**, 2979–2996 (2015).
37. Tamarin, T. & Kaspi, Y. The poleward motion of extratropical cyclones from a potential vorticity tendency analysis. *J. Atmos. Sci.* **73**, 1687–1707 (2016).
38. Tamarin, T. & Kaspi, Y. Mechanisms controlling the downstream poleward deflection of midlatitude storm tracks. *J. Atmos. Sci.* **74**, 553–572 (2017).
39. Vallis, G. K. *Atmospheric and Oceanic Fluid Dynamics*. (Cambridge University Press, Cambridge, UK, 2006).
40. Stoelinga, M. T. A potential vorticity-based study of the role of diabatic heating and friction in a numerically simulated baroclinic cyclone. *Mon. Weath. Rev* **124**, 849–874 (1996).

41. Barnes, E. A. & Polvani, L. Response of the midlatitude jets, and of their variability, to increased greenhouse gases in the CMIP5 Models. *J. Clim.* **26**, 7117–7135 (2013).
42. Held, I. M. & Soden, B. J. Robust responses of the hydrological cycle to global warming. *J. Clim.* **19**, 5686–5699 (2006).
43. Yettella, V. & Kay, J. E. How will precipitation change in extratropical cyclones as the planet warms? Insights from a large initial condition climate model ensemble. *Clim. Dyn.* **49**, 1769–1781 (2016).

Acknowledgements

The data were obtained from the World Data Center for Climate (WDCC). We acknowledge the World Climate Research Programmes Working Group on Coupled Modelling, which is responsible for CMIP, and we thank the climate modelling groups (listed in Supplementary Table 1 and Supplementary Data) for producing and making available their model output. For CMIP, the US Department of Energy's Program for Climate Model Diagnosis and Intercomparison provides coordinating support and led development of software infrastructure in partnership with the Global Organization for Earth System Science Portals. The authors also thank K. Hodges for providing the tracking algorithm and his help with implementing it on the CMIP5 data. We also thank B. Stevens and M. Esch from the Max-Planck Institute for Meteorology, for providing the high-temporal-resolution data necessary for the PV analysis. This research has been supported by the Israeli Science Foundation (grant 1819/16).

Author contributions

T.T.-B. and Y.K. designed the study and wrote the paper; T.T.-B. performed the data analyses.

Competing interests

The authors declare no competing financial interests.

Additional information

Supplementary information is available for this paper at https://doi.org/10.1038/s41561-017-0001-8.

Reprints and permissions information is available at www.nature.com/reprints.

Correspondence and requests for materials should be addressed to T.T.-B

Methods

Tracking algorithm. The objective feature-tracking algorithm used here is that of Hodges[35]. We use the 850 hPa zonal and meridional velocities to compute the relative vorticity field, and identify the cyclones as maxima of vorticity. Each CMIP5 model is smoothed on a T42 grid by removing spatial wavenumbers larger than 42 and smaller than 5, so both the small-scale noise and the large-scale background flow are removed. This also makes the comparison between models of different horizontal resolution easier. A cutoff of $10^{-5}\,s^{-1}$ is used to identify the vorticity features, and their centres are then tracked every six hours. The tracking involves minimizing a cost function for the track smoothness, by restricting changes in speed and propagation[35]. Only cyclones that have a lifetime greater than two days and that propagate distances larger than 1,000 km are kept for further analysis, to eliminate stationary or spurious cyclones. The results presented here do not change qualitatively if these requirements are relaxed or if sea-level pressure systems are tracked instead.

Data availability. The data sets analysed in the current study were obtained from the World Data Center for Climate (WDCC) repository, and are available at http://cera-www.dkrz.de/WDCC/ui/.

Code availability. The code of K. I. Hodges[35] that was used to generate the tracking results is available at http://www.nerc-essc.ac.uk/~kih/TRACK/Track.html.